*Int. J. Electrochem. Sci.*, 16 **(2021)** Article ID: 210943, doi: 10.20964/2021.09.26

International Journal of
ELECTROCHEMICAL
SCIENCE
www.electrochemsci.org

# Direct Electrooxidation Synthesis of Nickel Hypophosphite and Its Application in Electroless Nickel Plating

*Wanmin Liu*[*], *Wen Xu, Mulan Qin, Weigang Wang, Bin Shen, Lv Xu*

Hunan Provincial Key Laboratory of Environmental Catalysis & Waste Recycling, College of Materials and Chemical Engineering, Hunan Institute of Engineering, Xiangtan 411104, China
[*]E-mail: william@hnie.edu.cn

*Received:* 29 April 2021 / *Accepted:* 2 July 2021 / *Published:* 10 August 2021

The polarization curve and cyclic voltammetry techniques were used to investigate the electrochemical behavior of nickel in the hypophosphorous acid solution. Nickel hypophosphite synthesized by the direct electrooxidation method was directly used for electroless nickel plating. The morphology, phosphorus content, structure and corrosion resistance of the as-prepared nickel deposition were characterized by scanning electron microscopy, energy-dispersive X-ray spectroscopy, X-ray diffraction, polarization curve and electrochemical impedance spectroscopy. The results show that the anodic oxidation process of nickel in the hypophosphorous acid solution consists of active, active-passive, passive, transpassive and oxygen evolution regions. The electrolyte with a $Ni^{2+}$ concentration of 8.07 $g \cdot L^{-1}$ and the molar ratio of 0.36 for $Ni^{2+}/H_2PO_2^-$ is obtained by controlling the anodic potential at 0.24 V for 3 h in 25 $g \cdot L^{-1}$ hypophosphorous acid solution. Compared to the industrial nickel deposition, the nickel plating layer got from the bath containing the above electrolyte has more compact surface, higher phosphorus content and better corrosion resistance.

**Keywords:** hypophosphorous acid; nickel hypophosphite; direct electrooxidation; electroless nickel plating; corrosion resistance

## 1. INTRODUCTION

In industry, nickel sulphate ($NiSO_4$)-sodium hypophosphite ($NaH_2PO_2$) system is usually used as the electroless nickel plating solution, which consists of nickel sulphate, sodium hypophosphite, complexing agent, stabilizing agent and other additives. As the plating process progresses, $SO_4^{2-}$, $Na^+$ and $H_2PO_3^-$ accumulate gradually, causing the solution to be discarded. It is reported that the treatment of the spent solution is extremely troublesome [1-4]. Therefore, a nickel

hypophosphite ($(Ni(H_2PO_2)_2)$) - hypophosphorous acid ($H_3PO_2$) system, using $Ni(H_2PO_2)_2$ as the main salt/reducing agent and $H_3PO_2$ as the auxiliary reducing agent, was reported in our previous work. The plating layer, bath performance and lifetime of this system are superior to those of the $NiSO_4$-$NaH_2PO_2$ system [5]. Especially, the waste solution can be directly used as a raw material to synthesize one kind of multi-doped lithium iron phosphate cathode for lithium-ion batteries with excellent electrochemical properties [6-9]. Thus, $Ni(H_2PO_2)_2$ can be the better raw material for electroless nickel plating, owing to the provision of $Ni^{2+}$ and $H_2PO_2^-$ without the introduction of $SO_4^{2-}$ and $Na^+$, which contributes to the enhancement of the plating layer and the bath properties, as well as the resource utilization of the waste solution.

Nowadays, $Ni(H_2PO_2)_2$ has been prepared by various ways, such as double decomposition, acid-base neutralization, ion exchange and electrolytic route. The double decomposition method is characterized by easy operation but low-purity product, using $Ni(NO_3)_2$ and $NaH_2PO_2$ as raw materials [10]. In the acid-base neutralization method, $Ni(H_2PO_2)_2$ is obtained by the reaction of $H_3PO_2$ with $NiCO_3$ or $Ni(OH)_2$, marked by higher purity and cost [11]. In addition, $Ni(H_2PO_2)_2$ can be gained from the exchange reaction between $Ni^{2+}$ and $H^+$ by the ion exchange technique [11], where the cationic exchange resin was immersed in the solutions containing high concentration of $Ni^{2+}$ and $H_3PO_2$ in sequence. This route has the characteristics of the highest purity but the lowest production efficiency. The electrolytic method is carried out in three or four-compartment electrodialysis cell, with $NiSO_4$ and $NaH_2PO_2$ as the raw materials, and nickel slice or other insoluble electrodes as the anodes. Although high-purity $Ni(H_2PO_2)_2$ can be generated, the cost is higher by virtue of complicated equipments in the process [10]. From the above analyses, it can be seen that these above-mentioned preparation methods have disadvantages to some extent.

In the present study, the polarization curve and cyclic voltammetry technique were firstly applied to investigate the electrochemical behavior of the nickel electrode in $H_3PO_2$ solution, followed by the synthesis of $Ni(H_2PO_2)_2$ through the direct electrooxidation method with advantages of easy operation, low price and no diaphragm. Then, the obtained electrolyte containing $Ni(H_2PO_2)_2$ and $H_3PO_2$ was directly used for electroless nickel plating and the as-prepared nickel layer was characterized with all sorts of techniques. To the best of our knowledge, this route has not been reported.

## 2. EXPERIMENTAL

### *2.1 Experimental process*

ⅰ) Electrochemical behavior of the nickel electrode in $H_3PO_2$ solution

The three-electrode system was composed of a nickel electrode, a platinum foil and a saturated calomel electrode (SCE), which were used as the working electrode, the auxiliary electrode and the reference electrode, respectively. The working electrode was encapsulated with epoxy resin, leaving the areas of 1 $cm^2$ to exposure to 25 $g \cdot L^{-1}$ $H_3PO_2$ solution at 25 ℃. The polarization curve and cyclic voltammetry (CV) curve were measured on an electrochemical

workstation (AUTOLAB PGSTAT302N) at scan rates of 0.1 and 50 $mV \cdot s^{-1}$ in the ranges of -0.50~1.80 and -0.25~0.75 V, respectively. All the potentials described in the paper were with respect to the SCE.

ⅱ) Synthesis of $Ni(H_2PO_2)_2$

$Ni(H_2PO_2)_2$ was prepared through a direct electrooxidation method by controlling the anodic potential at 0.24 V for different electrolysis time at 25 ℃, using $H_3PO_2$ solutions with different concentration as the electrolyte, a nickel slice (40 mm × 30 mm × 5mm) and a platinum foil (40 mm × 30 mm × 1mm) as the anode and the cathode, respectively. The as-prepared $Ni(H_2PO_2)_2$ and remaining $H_3PO_2$ in electrolyte solution were directly used for electroless nickel plating.

ⅲ) Electroless nickel plating

The electroless nickel plating process was finished on the Q235 steel substrate in the $Ni(H_2PO_2)_2$-$H_3PO_2$ system under the temperature of 90 ℃, the time of 1 h and the pH value of 4-5, with mechanical agitation and the loading capacity of 1 $dm^2 \cdot L^{-1}$. The system consisted of the above as-prepared $Ni(H_2PO_2)_2$ and $H_3PO_2$ electrolyte solution containing 8.07 $g \cdot L^{-1}$ $Ni^{2+}$, 20 $g \cdot L^{-1}$ lithium acetate, 20 $g \cdot L^{-1}$ citric acid and 1.5 $g \cdot L^{-1}$ maleic acid (marked by ENS1). For comparison, the $NiSO_4$-$NaH_2PO_2$ system applied in the industry was also used for electroless nickel plating under the same technological condition, which was composed of 30 $g \cdot L^{-1}$ nickel sulfate, 20 $g \cdot L^{-1}$ sodium hypophosphite, 20 $g \cdot L^{-1}$ sodium acetate, 20 $g \cdot L^{-1}$ sodium citrate and 1.5 $g \cdot L^{-1}$ maleic acid (marked by ENS2). The obtained nickel plating layers from two systems were named ENL1 and ENL2, separately.

### *2.2 Performance characterization*

The content of $Ni^{2+}$ was analyzed by the EDTA titration method using murexide as the indicator. The content of $H_2PO_2^-$ was determined by the iodometry method. The deposition rate was measured by the gravimetrical method. The thickness measurement was carried out by a digital micrometer before and after plating. The bending test of the nickel plating layer on the substrate was performed by an adhesion tester (PosiTest AT-M). The surface morphology, phosphorus content and structure of the nickel plating layer were examined by scanning electron microscopy (SEM; JEOL, JSM-6360LV), energy-dispersive X-ray spectroscopy (EDS) and X-ray diffraction (XRD; D/max-rA-type Cu-$K_\alpha$; 40kV, 300 mA and 10-80 ℃), respectively. The corrosion resistance of samples in the 3.5 wt.% NaCl solution was evaluated by the polarization curve in the range of -0.80~-0.10 V and electrochemical impedance spectroscopy (EIS) performed on the electrochemical workstation over the frequency range of $10^{-2}$-$10^6$ Hz with the amplitude of ±5 mV.

## 3. RESULTS AND DISCUSSION

### *3.1 Determination of electrolyzation potential*

Fig. 1 shows the polarization curve of the Ni electrode in $H_3PO_2$ solution. It is easily found that the curve is composed of cathodic and anodic zones. When the electrode is cathodically polarized, continuous $H_2$ bubbles are released, accompanying the occurrence of the hydrogen evolution reaction ($2H^+ + 2e \rightarrow H_2$) shown at ab segment (-0.5000 ~ -0.2938 V). The anodic polarization curve can be divided into active, active-passive, passive, transpassive and oxygen evolution zones. In the active region (bc segment, -0.2938 ~ 0.2938 V), the current density increases with the positive movement of the electrode potential, corresponding to the dissolution reaction of the Ni electrode ($Ni - 2e \rightarrow Ni^{2+}$). In the active-passive region (cd segment, 0.2938 ~ 0.4349 V), the current density decreases dramatically with the increase of the electrode potential, suggesting the transfer of the active state into the passive state owing to the formation of NiO on the surface of the Ni electrode.

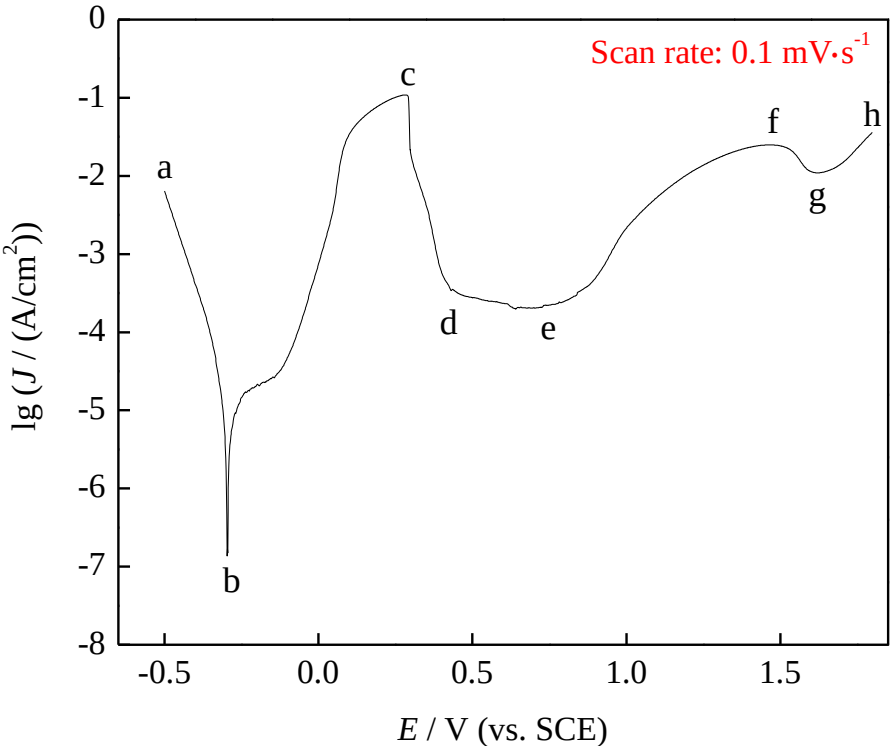


**Figure 1**. Polarization curve of the nickel electrode in 25 $g \cdot L^{-1}$ hypophosphorous acid.

When the potential moves to 0.4349 ~ 0.7376 V (de segment), the current density stays at ~ $10^{-4}$ $A \cdot cm^{-2}$, indicating extremely slow dissolution velocity of the Ni electrode in the passive region. As the potential extends to 0.7376 ~ 1.6192 V (eg segment), the current density augments again with the further anodic polarization. This may be attributed to the emergence of a new electrode reaction ($Ni^{2+} - e \rightarrow Ni^{3+}$) which damages the passive film and hence induces the re-

enlargement of the dissolution rate of the Ni electrode. Once the potential reaches above 1.6192 V, the oxygen evolution reaction ($2H_2O \rightarrow 4H^+ + O_2 + 4e$) takes place. These experimental phenomena are similar with the electrochemical behavior of Ni in acidic chloride solution or Fe-Ni alloy in sulfuric aicd solution [12-13]. From the above analyses, it can be concluded that the potential range of -0.2938 ~ 0.2938 V is appropriate for the synthesis of $Ni(H_2PO_2)_2$ by the direct electrooxidation method.

Fig. 2 exhibits the CV curve of the Ni electrode in $H_3PO_2$ solution. It is obvious that during the process of positive scan, the oxidation current appears at -0.1119 V, followed by an oxidation peak at 0.2383 V with the maximum current. Then, the oxidation current diminishes rapidly and disappears at 0.3730 V. This is because Ni begins to dissolve at -0.1119 V in $H_3PO_2$ solution, with the maximum dissolution velocity of 0.0635 $A \cdot cm^{-2}$ at 0.2383 V. However, Ni doesn't dissolve after 0.3730 V. Additionally, no reduction peak is found when the scan direction is altered, suggesting the irreversible characteristic of the electrochemical oxidation of Ni [14-15]. These results are in accordance with those of the polarization curve investigation. Therefore, the potential of about 0.24 V is suitable for electrosynthesizing $Ni(H_2PO_2)_2$ in order to reach the maximum reaction rate.

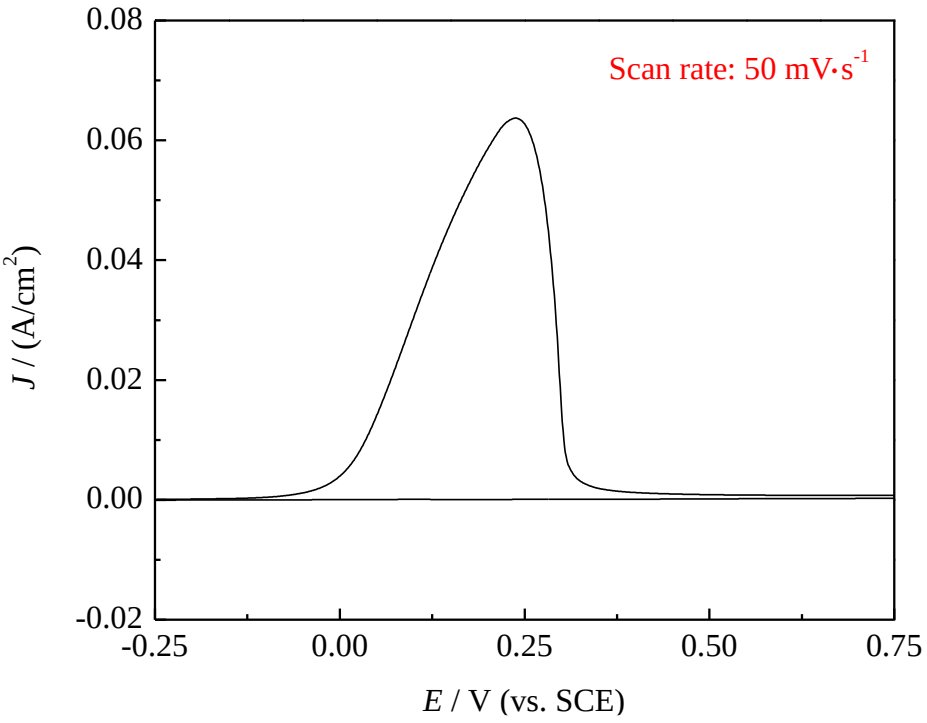


**Figure 2.** CV curve of the nickel electrode in 25 $g \cdot L^{-1}$ hypophosphorous acid.

### *3.2 Direct electrosynthesis of $Ni(H_2PO_2)_2$*

The experimental results of $Ni(H_2PO_2)_2$ prepared by the direct electrooxidation method are displayed in table 1. As can be seen from the table, with the extension of electrolysis time in

solution with the same $H_3PO_2$ concentration , the concentration of $Ni^{2+}$ increases, the content of $H_2PO_2^-$ is unchanged and no $O_2$ bubbles are released. On the other hand, if the electrolysis is manipulated for the same time in solutions with different $H_3PO_2$ concentration, only the content of $Ni^{2+}$ significantly ascends with the increase of $H_3PO_2$. As we know, there exist three possible oxidation reactions ($Ni - 2e \rightarrow Ni^{2+}$, $E^0(Ni|Ni^{2+}) = 0.25$ V; $H_3PO_2 + H_2O - 2e^- \rightarrow H_3PO_3 + 2H^+$, $E^0(H_3PO_2|H_3PO_3) = 0.499$ V; $2H_2O - 4e \rightarrow 4H^+ + O_2$, $E^0(H_2O|O_2) = 1.229$ V [16]) at the anodic electrode in this electrochemical system. The electrode reaction with the lowest deposition potential preferentially takes place at the anode. As a result, only Ni is oxidated during the course of the electrolysis, accompanying the change of $Ni^{2+}$ concentration. A number of references reported that the nickel plating layer with excellent properties can be gained when the mole ratio of $Ni^{2+}$ to $H_2PO_2^-$ is in the range of 0.3-0.45 and the content of $H_2PO_2^-$ is about 23 $g \cdot L^{-1}$ in the plating bath [17-20]. Therefore, the electrolyte containing 8.07 $g \cdot L^{-1}$ $Ni^{2+}$ and 24.62 $g \cdot L^{-1}$ $H_2PO_2^-$ can be directly used for electroless nickel plating, which is obtained through electrolyzation for 3 h in 25 $g \cdot L^{-1}$ $H_3PO_2$ solution.

**Table 1.** Results of $Ni(H_2PO_2)_2$ prepared by the direct electrooxidation method.

| $\rho(H_3PO_2)$ /($g \cdot L^{-1}$) | $t$/h | $\rho(Ni^{2+})$ /($g \cdot L^{-1}$) | $\rho(H_2PO_2^-)$ /($g \cdot L^{-1}$) | $n(Ni^{2+})$ :$n(H_2PO_2^-)$ | Current efficiency/% |
|---|---|---|---|---|---|
| 10 | 1 | 1.26 | 9.85 | 0.14 | 26.59 |
| 10 | 3 | 2.12 | 9.85 | 0.24 | 14.32 |
| 10 | 5 | 3.96 | 9.85 | 0.45 | 15.45 |
| 25 | 1 | 3.85 | 24.62 | 0.17 | 80.36 |
| 25 | 3 | 8.07 | 24.62 | 0.36 | 54.28 |
| 25 | 5 | 9.73 | 24.62 | 0.44 | 40.12 |
| 50 | 1 | 7.92 | 49.24 | 0.18 | 88.79 |
| 50 | 3 | 14.66 | 49.24 | 0.33 | 54.63 |
| 50 | 5 | 20.01 | 49.24 | 0.45 | 43.47 |

*3.3 Performance characterization of the nickel plating layer*

Electroless nickel plating is an autocatalytic process achieved by immersion of a substrate in a plating bath. The nickel plating layer can be deposited according to equation (1) [21-25], whether in the ENS1 or in the ENS2.

$$Ni^{2+} + 4H_2PO_2^- + H_2O - 3e \rightarrow Ni + P + 3H_2PO_3^- + 2H^+ + H_2 \quad (1)$$

The biggest difference is that there is sodium sulphate in the ENS2, while no sodium sulphate in the ENS1. Consequently, the latter can rule out the effect of sodium sulphate, which is expected to enhance the performance of the plating solution and nickel deposition.

The SEM images of ENL1 and ENL2 are presented in Fig. 3. There exist continuous uniform small particles with the size of 1 μm and there is no clear grain boundary among the

particles on the compact surface of ENL1. Comparatively, the dimension of the particles on ENL2 is bigger than that on ENL1, with tiny crystal boundary. The gravimetrical method proves that the average deposition rate of the first ten times is 14.21 μm·h$^{-1}$, higher than that of ENL2 (11.76 μm·h$^{-1}$). The thickness of ENL1 (13.96 μm) of the tenth time is bigger than that of ENL2 (11.23 μm). Simultaneously, ENL1 and ENL2 show excellent adhesion strength with the substrate, with the adhesive force of approximately 2.77 MPa and 2.75 MPa for ENL1 and ENL2, respectively. These morphology, deposition rate, thickness and adhesive force differences may mainly be related to the components of plating bath system. Generally, a relatively high temperature is one of the prerequisites that ensure the occurrence of the electroless plating process. The diffusion rate of ions from the solution to the substrate is far higher than their consumed rate on the depositing surface at relatively high temperature. As a result, the ions involved electrochemical reactions can be compensated immediately, while those ions in the solution can be treated as a constant state. Thus, the electron transfer step happened between $Ni^{2+}$ and $H_2PO_2^-$ to form Ni-P layer on the substrate is the rate controlled step [26]. In addition, the activation energy is a key factor influencing the nickel deposition rate and it mainly refers to that for growth of the Ni-P layer [26-27]. Taking into account the components of the two kinds of plating bathes, ENS1 ruled out the influence of $Na^+$ and $SO_4^{2-}$ in comparison with ENS2, which may be contributed to the diffusion of $Ni^{2+}$ and $H_2PO_2^-$ and the decrease of reaction activation energy in ENS1. These factors gave rise to higher deposition rate, bigger thickness, denser surface and stronger adhesive force of ENL1.

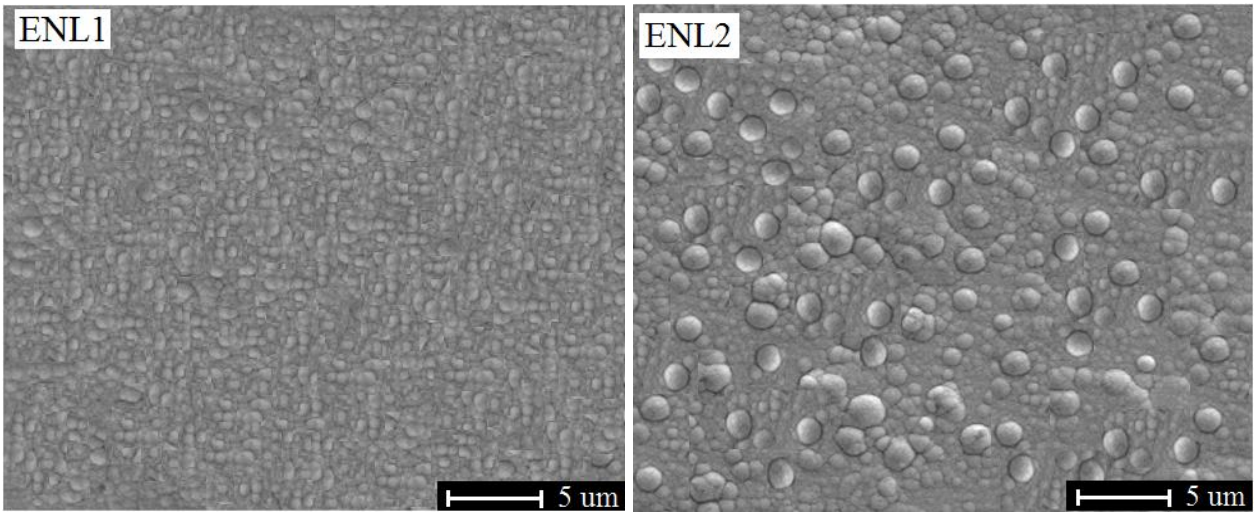


**Figure 3.** SEM images of ENL1 and ENL2.

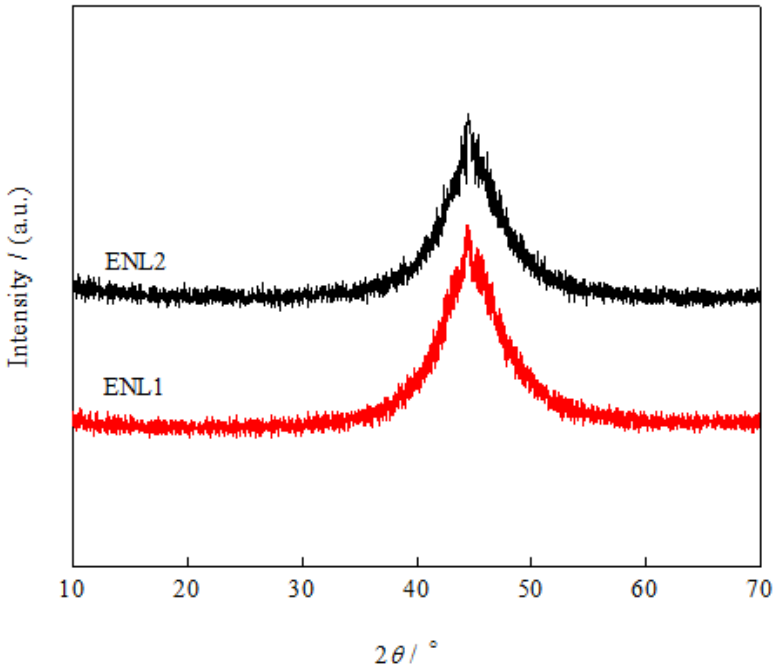


**Figure 4.** XRD patterns of ENL1 and ENL2.

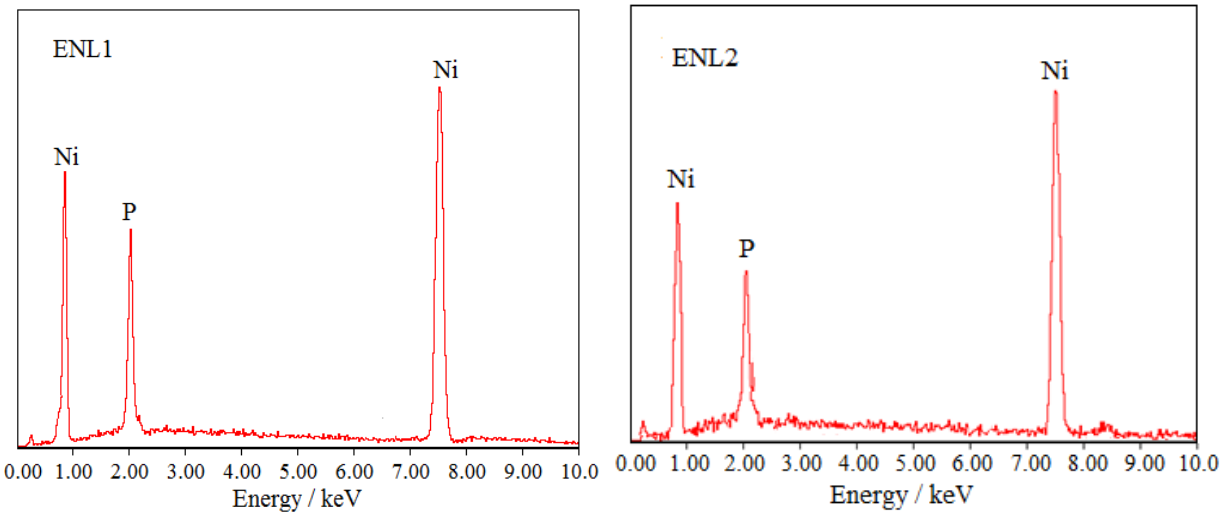


**Figure 5.** EDS curves of ENL1 and ENL2.

To confirm structural characterization of the electroless plated Ni-P solid solution alloy, XRD analyses of the samples were carried out, as shown in Fig. 4. In the XRD patterns of ENL1 and ENL2, a broad diffraction peak at around 45° with a low intensity is apparently found, which indicates that ENL1 and ENL2 are amorphous. It has been measured that only amorphous Ni-P solid solution structure can be formed for the alloy with high P composition (>10%) [28-29]. The EDS curves of ENL1 and ENL2 in Fig. 5 showed that the two kinds of nickel deposits consist of nickel and phosphorus elements without other impurities, and the phosphorus content is 13.19 wt.% and 10.84 wt.% for ENL1 and ENL2, respectively.

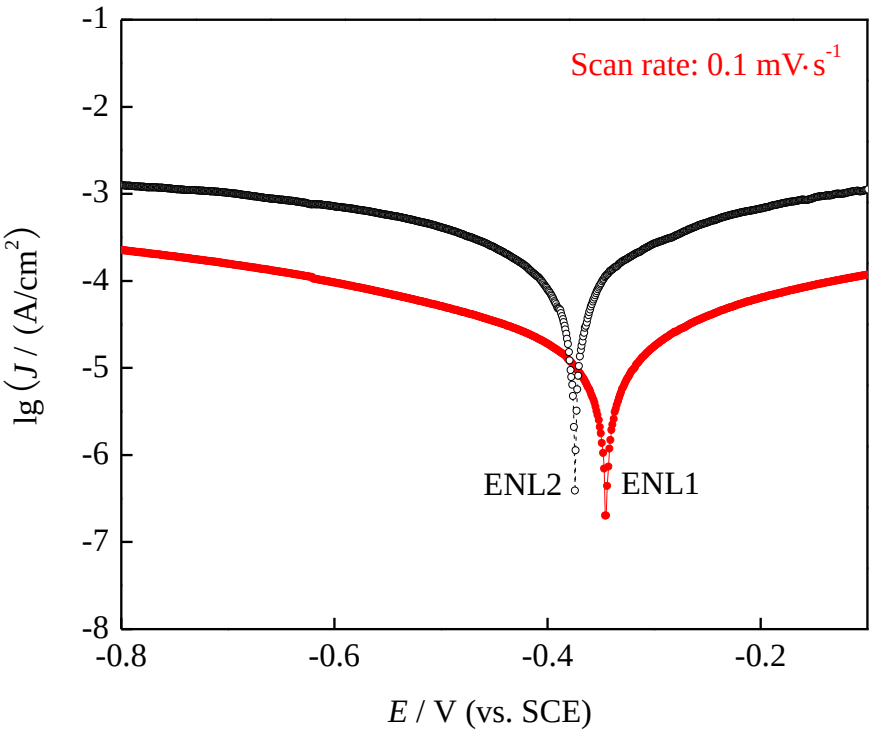


**Figure 6.** Polarization curves of ENL1 and ENL2 in 3.5 wt.% NaCl solution.

To investigate the corrosion resistance of ENL1 and ENL2, potentiodynamic polarization tests were performed. The representative polarization curves are displayed in Fig. 6. The corrosion potential and corrosion current density are extracted from polarization curves through extrapolating the linear portions of curves. The corrosion potential of ENL1 is -337.6 mV, higher than that of ENL2 (-373.2 mV). While the corrosion current density of ENL1 is $7.59\times10^{-7}$ A·cm$^{-2}$, lower than that of ENL2 ( $8.42\times10^{-6}$ A·cm$^{-2}$). This testifies that the corrosion resistance of the plating layer got from $Ni(H_2PO_2)_2$-$H_3PO_2$ system is better than that obtained from the industrial plating solution ($NiSO_4$-$NaH_2PO_2$ system), which attributes to the denser surface, higher phosphorous content, bigger thickness and stronger adhesive force of the former.

In order to further interpret the corrosion resistance of ENL1 and ENL2, EIS measurements were conducted, as shown in Fig. 7. It is observed that both of the curves are composed of the capacitive semicircles at the intermediate frequency and the inclined lines at the low frequency. The capacitive semicircles are related to the electrochemical arrangement between the electric-double layer capacitance and the charge transfer resistance [30]. The diameter of the semicircle, signifying the charge transfer resistance of the electrode/solution interface ($R_{ct}$), can be used to assess the corrosion resistance of the plating layer [31]. The bigger the $R_{ct}$ value is, the better the corrosion resistance is. The $R_{ct}$ value of ENL1 is $1.91\times10^4$ Ω·cm$^2$, higher than that of ENL2 ($1.42\times10^4$ Ω·cm$^2$), indicating superior corrosion resistance of ENL1 to that of ENL2. The result of charge transfer resistance is in good agreement with the polarization curve result.

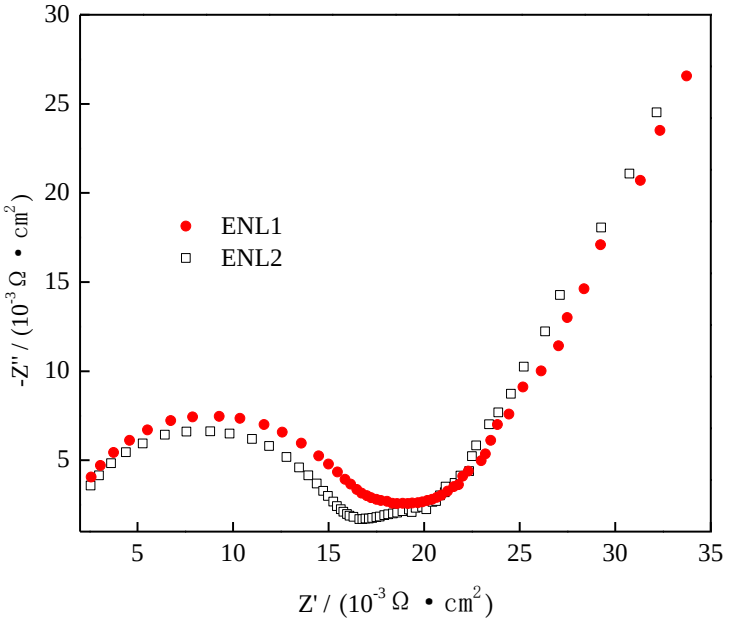


**Figure 7.** EIS curves of ENL1 and ENL2 in 3.5 wt% NaCl solution.

## 4. CONCLUSIONS

The polarization curve revealed that the anodic oxidation process of nickel in the hypophosphorous acid is composed of activation, activation-passivation, passivation, transpassivation and oxygen evolution regions. The cyclic voltammetry technique determined the optimum potential of 0.24 V for the direct electrooxidation synthesis of nickel hypophosphite. Nickel hypophosphite was directly synthesized by a potentiostatic electrolysis method, which was performed at 0.24 V for 3 h in 25 $g \cdot L^{-1}$ hypophosphorous acid at 25 ℃, with a nickel slice and a platinum foil as the anode and the cathode, respectively. The obtained electrolyte with a $Ni^{2+}$ concentration of 8.07 $g \cdot L^{-1}$ and the molar ratio of 0.36 for $Ni^{2+}/H_2PO_2^-$ was used as a main salt and reducing agent for electroless nickel plating. The as-prepared nickel layer showed uniform and smooth appearance with compact tiny particles, amorphous structure with high phosphorus content, good adhesion and excellent corrosion resistance.

ACKNOWLEDGEMENTS
This work was supported by the Scientific Research Fund of Hunan Provincial Education Department, China (19A111), the Provincial Natural Science Foundation of Hunan, China (2020JJ5102 ).

## References

1. Y. Shih, C. Lin and Y. Huang, *Sep. Purif. Technol.*, 100 (2013) 104.
2. P. Liu, C. Li, X. Liang, G. Lu, J. Xu, X. Dong, W. Zhang and F. Ji, *Green Chem.*, 16 (2014)

1217.
3. L. Li, N. Takahashi and K. Kaneko, *Sep. Purif. Technol*., 147 (2015) 237.
4. G. Chen, W. Sun, Q. Wu, Y. Kong and Z. Xu, *J. Appl. Polym. Sci.*, 134 (2017) 45049.
5. W. Liu, Q. Liu, L. Xu, M. Qin and J. Deng, *Surf. Rev. Lett*., 26 (2019) 1850130.
6. W. Liu, Q. Huang and G. Hu, *J. Alloys Comp*., 632 (2015) 185.
7. Q. Liu, W. Liu, D. Li, H. Chen and Z. Wang, *Electrochim. Acta*, 184 (2015) 143.
8. Q. Liu, W. Liu, D. Li and Z. Wang, *Mater. Lett*., 162 (2016) 87.
9. W. Liu, Q. Liu, M. Qin, L. Xu and J. Deng, *Electrochim. Acta*, 257 (2017) 82.
10. Y. Zhang, Z. Zhong, A. Guo, C. Wang, X. Fu and B. Zhang, *Acta Scientiarum Naturalium Universitatis Nankaiensis*, 35 (2002) 80.
11. G. Jeanneret, P. Bruner and D. Jousset, United States patent US, 6,030,593. 2000 Feb 29.
12. M. Zamin and M. B. Ives, *J. Electrochem. Soc.*, 121 (1974) 1141.
13. G. Economy, *J. Electrochem. Soc.*, 108 (1961) 337.
14. W. Liu, G. Hu, X. Xiao, P. Zhong and L. Xu, *J. Cent. South Univ.*, 43 (2012) 842.
15. J. Heinze, *Angew. Chem. Int. Ed. Engl.*, 23 (1984) 831.
16. D. Li, Electrochemical principles, Beijing University of Aeronautics and Astronautics Press, (2018) Beijing, China.
17. K. U. V. Kiran, A. Arora, B. R. Sunil and R. Dumpala, *SN Appl. Sci*., 2 (2020) 1101.
18. P. R. Deshmukh, H. S. Hyun, Y. Sohn, W. G. Shin, *Korean J. Chem. Eng*., 37 (2020) 546.
19. F. G. Whyte, V. S. Aigbodion, G. M. Whyte and I. C. Ezema, *J. Bio- Tribo-Corros*., 6 (2020) 137.
20. A. M. Abioye, L. N. Abdulkadir and F. N. Ani, *J. Electronic Mater*., 48 (2019) 3721.
21. A. V. Takaloo and S. K. Joo, *J. Korean Phys. Soc*., 72 (2018) 615.
22. P. Verdi and S. M. Monirvaghefi, *J. Mater. Eng. Perform*., 29 (2020) 7915.
23. M. K. Pal, G. Gergely, D. K. Hrvath and Z. Gacsi, *Powder Metall. Met. Ceram*., 58 (2020) 529.
24. Q. Qi, Y. Wang, X. Ding, W. Wang, R. Xu and D. Yu, *Appl. Organomet Chem*., 34 (2020) 5434.
25. Z. Wang, T. Li, J. Yu, Z. Hu, J. Zhu and Y. Wang, *Adv. Eng. Mater*., 21 (2019) 1801041.
26. M. Fang, L. Hu, L. Yang, C. Shi, Y. Wu and W. Tang, *Trans. Nonferrous Met. Soc. China*, 26 (2016) 799.
27. W. Wu and J. Jiang, *Appl. Nanosci*., 7 (2017) 325.
28. T. Hentschel, D. Isheim, R. Kirchheim, F. Muller and H. Kreye, *Acta Materialia*, 48 (2000) 933.
29. H. Wang, L. Liu and W. Jiang, *Trans. Nonferrous Met. Soc. China*, 24 (2014) 3014.
30. J. A. Calderon, J. E. Henao and M. A. Gomez, *Electrochim. Acta*, 124 (2014) 190.
31. S. Chen, Q. Zhu, Y. Zhao, J. He and G. Wang, *Mater. Corros*., 70 (2019) 720.